ACS NANO

www.acsnano.org

Downloaded via UNIV SCIENCE AND TECHNOLOGY BEIJING on December 12, 2025 at 08:25:12 (UTC).
See https://pubs.acs.org/sharingguidelines for options on how to legitimately share published articles.

Enhanced In-Plane Thermal Conductance of Thin Films Composed of Coaxially Combined Single-Walled Carbon Nanotubes and Boron Nitride Nanotubes

Pengyingkai Wang, Yongjia Zheng, Taiki Inoue,* Rong Xiang, Ahmed Shawky, Makoto Watanabe, Anton Anisimov, Esko I. Kauppinen, Shohei Chiashi, and Shigeo Maruyama*

Cite This: *ACS Nano* 2020, 14, 4298−4305

Read Online

ACCESS | Metrics & More | Article Recommendations | Supporting Information

ABSTRACT: Carbon nanotubes (CNTs) and boron nitride nanotubes (BNNTs) are one-dimensional materials with high thermal conductivity and similar crystal structures. Additionally, BNNTs feature higher thermal stability in air than CNTs. In this work, a single-walled carbon nanotube (SWCNT) film was used as a template to synthesize a BNNT coating by the chemical vapor deposition (CVD) method to form a coaxial heterostructure. Then, a contact-free steady-state infrared (IR) method was adopted to measure the in-plane sheet thermal conductance of the as-synthesized film. The heterostructured SWCNT−BNNT film demonstrates an enhanced sheet thermal conductance compared with the bare SWCNT film. The increase in sheet thermal conductance shows a reverse relationship with SWCNT film transparency. An enhancement of over 80% (from ~3.6 to ~6.4 $\mu W \cdot K^{-1} \cdot sq^{-1}$) is attained when the BNNT coating is applied to an SWCNT film with a transparency of 87%. This increase is achieved by BNNTs serving as an additional thermal conducting path. The relationship between the thermal conductance increase and transparency of the SWCNT film is studied by a structured modeling of the SWCNT film. We also discuss the effect of annealing on the thermal conductance of SWCNTs before BNNT growth. Along with the preservation of high electrical conductance, the enhanced thermal conductance of the heterostructured SWCNT−BNNT films makes them a promising building block for thermal and optoelectronic applications.

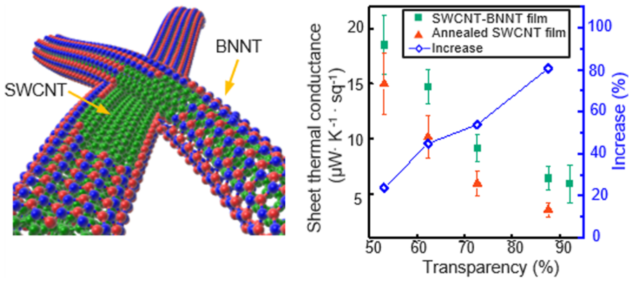

KEYWORDS: *single-walled carbon nanotube film, boron nitride nanotube, van der Waals heterostructure, in-plane sheet thermal conductance, chemical vapor deposition, infrared thermography*

In recent years, van der Waals heterostructures (vdWHs) consisting of different layers of materials weakly bounded to each other by van der Waals interactions have intrigued increasing interest. Using graphene as a basis, vdWHs started from two-dimensional (2D) heterostructures[1] (e.g., graphene, hexagonal boron nitride (BN), 2D metal chalcogenides, and 2D oxides) and developed into a larger field including one-dimensional (1D) heterostructures[2] (e.g., nanowires and nanoribbons) and integration of materials of different dimensions.[3] These vdWHs have been proven to feature unusual properties such as electrical, thermal, optical, and thermoelectric that were not observed previously.[4−8] These properties, which could be tailored, enable vdWHs materials readily applicable as functional materials and create various possible applications. The construction of heterostructures can be realized mainly by two strategies. One is a stacking method where prepared layers of different 2D nanomaterials are transferred on top of each other,[9,10] and the other is direct synthesis method in which target layers are grown on a starting material.[11,12] The layer-by-layer transfer is easily operated and the quality of the synthesized material is relatively high. However, the insufficient control on the structure parameters, undesired adsorption on the interfaces, and transfer-caused

Received: December 12, 2019
Accepted: April 9, 2020
Published: April 9, 2020

© 2020 American Chemical Society

https://dx.doi.org/10.1021/acsnano.9b09754

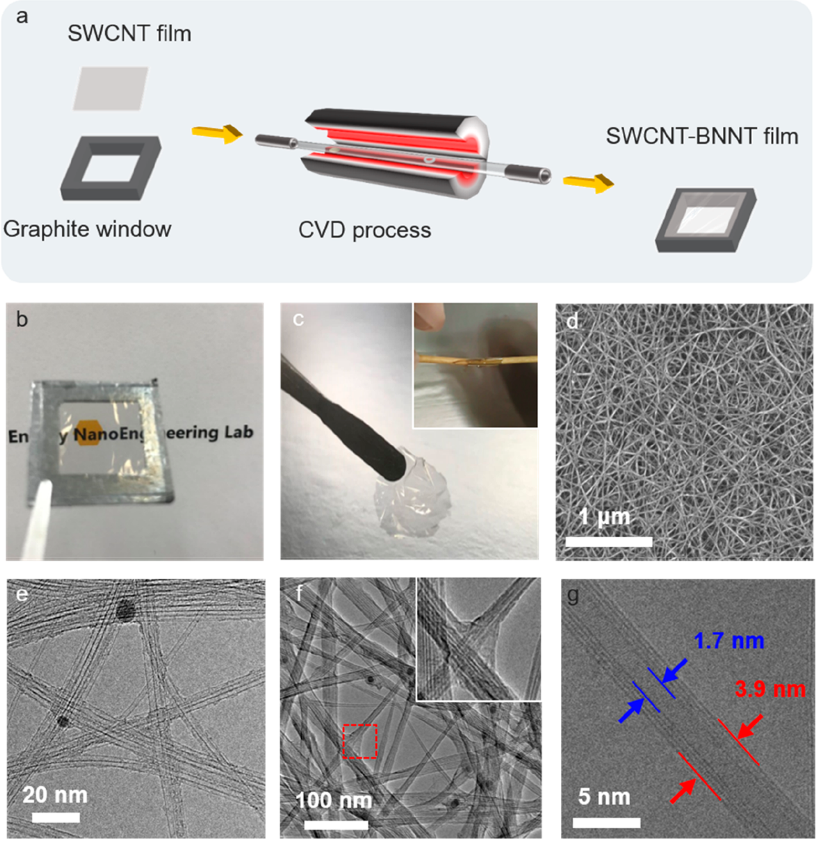

Figure 1. (a) Schematic of the CVD process for BNNT growth on an SWCNT template suspended on a graphite substrate. (b) Optical image of the SWCNT−BNNT heterostructured film (T87) suspended over a graphite window. Energy NanoEngineering Lab, permission granted. (c) Optical image of the SWCNT−BNNT film after it is rolled up (inset) and released, which confirms its spontaneous shape recovery. (d) SEM of the SWCNT−BNNT film. TEM images of (e) a bare SWCNT film and (f) the SWCNT film after being coated with BNNTs. (g) The TEM image of an isolated SWCNT coaxially coated by a three-wall BNNT. Diameters of the inner SWCNT and the outer triple-walled BNNT are 1.7 and 3.9 nm, respectively.

mechanical damages undoubtedly worsen their properties.[13,14] On the other hand, the synthesis method has attracted considerable attention due to its tunability and controllability. Among all the synthesis methods, chemical vapor deposition (CVD) technology has become a prevailing route to build the various heterostructures[5,7] owing to the high sample quality and outstanding scalability.[15] Compared with the transfer approach, CVD method is capable of preparing high-purity product with larger domain size and adjustable thickness.

A recent study used single-walled carbon nanotubes (SWCNTs) as a template and synthesized coaxial heterostructures by wrapping SWCNTs with boron nitride nanotubes (BNNTs) and molybdenum disulfide (MoS_2) nanotubes on each other by CVD process.[5] The synthesized BNNT is of high crystallinity and wraps the inner SWCNT uniformly and continuously. The well-crystallized surface and the tailored electrical property of BNNT give this heterostructure material chances in fabricating functional optoelectronic devices. The BNNT layer can also protect the inside SWCNT from oxidation. In another study, BNNT-wrapped SWCNT films were used as a high power-tolerant saturable absorber and are believed to have a significantly higher optical damage threshold as well as a great potential for various high-power optical applications.[7] Constructing heterostructures from BNNTs and CNTs is a promising way to combine the attracting properties of the two materials. Molecular dynamics simulations show that SWCNT−BNNT features good thermal stability and compressive resistance.[16] Experiments on measuring the out-of-plane thermal conductance of multiwalled carbon nanotube (MWCNT)−BNNT[17] array achieved a ~90% increase in thermal conductance compared with that of bare MWCNT arrays.[18] Besides CNT arrays, SWCNTs, which possess high thermal conductivity (~1000−5000 W $(m\cdot K)^{-1}$[19−22]), can also be assembled into random-network films. The 2D film is highly transparent and electrically conductive, which makes it a key player in solar cells working as a transparent electrode.[23,24] Therefore, it is of great interest to evaluate thermal, electrical, and other possible properties of heterostructured films made from SWCNT−BNNT.

In this study, the thermal property of the SWCNT−BNNT heterostructured films was studied experimentally, and the mechanism was discussed with a proposed model. The templates used are SWCNT films prepared by the aerosol CVD synthesis method[25] with variable transparency from 53% to 92%. The SWCNTs consisting of the films have uniformly small diameter, and the thickness of the films is controllable by altering the deposition time.[26] With the SWCNT films as a template, the heterostructured films were prepared by CVD, which can produce conformal and highly crystalline BNNTs.[5] Then, a contact-free steady-state infrared (IR) thermography measurement was used to investigate the in-plane sheet thermal conductance of the as-synthesized SWCNT−BNNT films. The sheet thermal conductance of the films before and after BNNT wrapping was measured and compared. An

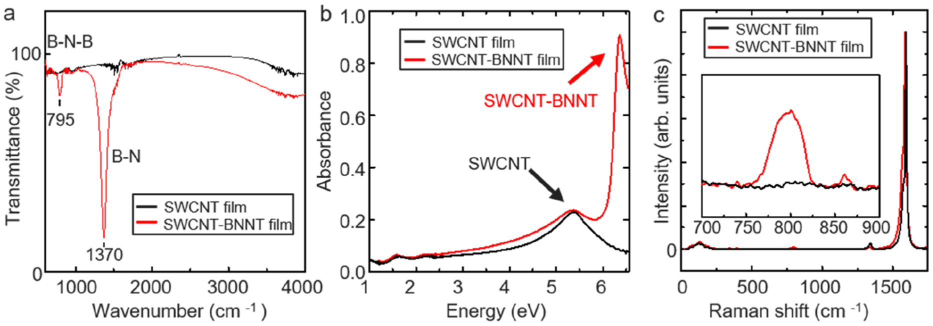

Figure 2. (a) FT-IR spectra, (b) UV−vis-NIR spectra, and (c) Raman spectra of SWCNT films before and after the BNNT coating was applied.

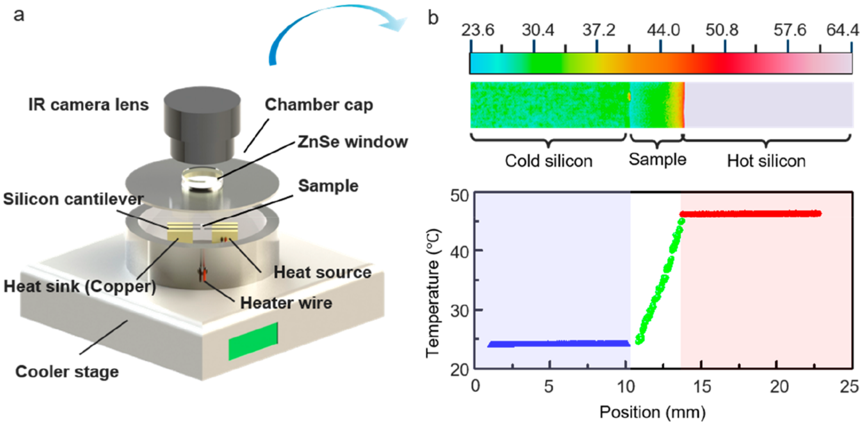

Figure 3. (a) Schematic of the experimental setup for the thermal conductance measurement. A temperature drop is generated by the heat source and heat sink. The chamber is kept under vacuum to eliminate convection. When the heat transport along the quasi-one-dimension reached a steady-state, the IR thermal imager recorded the temperature profiles for later analyses. (b) Upper: A typical thermal image of the temperature profile along the silicon−sample−silicon heat transfer. The emissivity is set to show the image of the sample, so the temperature of hot silicon exceeds the measurement range. Lower: The average temperature distribution on the silicon cantilevers (after emissivity correction) and the sample.

enhancement was observed for all samples measured at different degrees of transparency. On the basis of a concise model, the heat transfer mechanism in this heterostructured material and intertube contact effects were discussed.

RESULTS AND DISCUSSION

Preparation and Characterization of the SWCNT−BNNT Heterostructured Film. In this study, the five kinds of SWCNT film templates are denoted by their transparency at 550 nm, which was determined by their UV−vis-NIR spectra. In the following sections, these five samples are denoted as T53, T62, T72, T87, and T92, where T is the degree of transparency (%). UV−vis-NIR spectra and SEM images of these five SWCNT films are shown in Supporting Information, Figure S1. Figure 1a shows the two steps for synthesizing the SWCNT−BNNT film. First, the SWCNT template film was dry-transferred to a graphite substrate with a 1 cm × 1 cm window. Then, ammonia borane was used as the boron and nitrogen source and was sublimated by a heating belt after the temperature of the furnace increased to 1075 °C. With the suspended SWCNT film as a template, ammonia borane was carried by Ar/H_2 gas and deposited on the surface of SWCNTs to form a coaxial tube structure. In this way, heterostructured SWCNTs wrapped with BNNTs were prepared.[5] Figure 1b is an optical image of the as-synthesized heterostructured film (T87). BNNT adds obvious glossiness to the heterostructured film compared with the appearance of the bare SWCNT film (Supporting Information, Figure S2). After wrapped in BNNTs, the film retains its flexibility and can easily recover to the original morphology immediately when released, as shown in Figure 1c.[27] The SWCNT film easily rolls up but recovery to the original state is very difficult because the contacting surfaces adhere to each other. One possible explanation for this phenomenon is that the surface energy of the SWCNT film is very high (Supporting Information, Figure S3). The network morphology of the heterostructured film is shown in the scanning electron microscopy (SEM) image in Figure 1d. Figure 1e,f shows transmission electron microscopy (TEM) images of the SWCNT film before and after the BNNT coating is applied. No agglomeration is observed, and the walls of the tubes are clear and clean after BNNT growth. Suspended individual SWCNT or SWCNT bundles are fully coated by BNNTs, but at the junctions BN wrapped the whole junction rather than each SWCNT in the junction, as the inset shows in Figure 1f. The as-grown BNNT is multiwalled with an inner diameter determined by the size of the SWCNT or the SWCNT bundle template, as shown in Figure 1g. The outer diameter depends on the number of walls formed during CVD, and the number of walls can be controlled roughly by the CVD time. In this study, a 3 h CVD process resulted in BNNT growth of 2−10 walls. Figure 1g shows an isolated SWCNT coated by BNNTs with three walls. The distance between the walls of the BNNTs is about

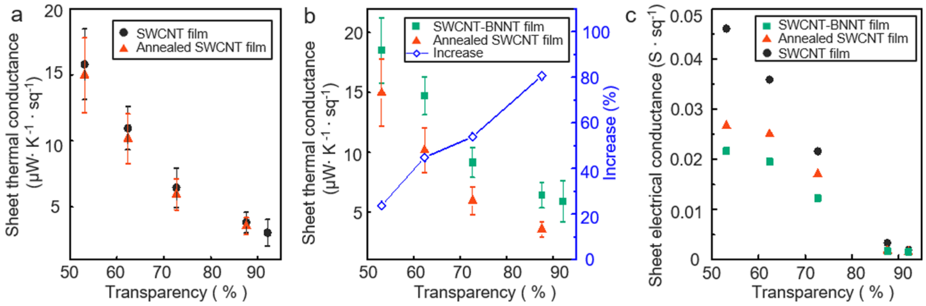

Figure 4. (a) Sheet thermal conductance of bare SWCNT films (black circle) and SWCNT films after annealing (orange triangle). A decrease is observed for all four samples measured after annealing. (b) Sheet thermal conductance (left axis) of SWCNT−BNNT films (mint square) and annealed SWCNT films (orange triangle). The blue hollow rhombuses show the increase ratio of the sheet thermal conductance after BNNT wrapping (right axis). (c) Sheet electrical conductance of bare SWCNT films (black circle), SWCNT films after annealing (orange triangle), and SWCNT−BNNT films (mint square).

0.36 nm, which is comparable to that of multiwalled BNNTs.[27,28]

For further characterization, Fourier transform infrared (FT-IR) spectra, UV−vis-NIR spectra, and Raman spectra (532 nm excitation wavelength) of the film were obtained before and after BNNT wrapping, as shown in Figure 2a−c, respectively. In Figure 2a, the signals of in-plane B−N stretching at 1370 cm $^{-1}$ and out-of-plane B−N−B bending at 795 cm $^{-1}$ are observed for the SWCNT−BNNT film, validating the existence of the B−N bond.[6,18,29] In the absorption spectra, a band gap of approximately 6 eV can be observed for BNNTs. This peak can be assigned to transitions due to the π−π^* bands of the BNNTs, which are consistent with Rubio's prediction.[30,31] The B−N−B bending mode at ~797 cm^{-1} is also observed in the Raman spectra in Figure 2c, as shown in the zoomed-in spectra, which further confirmed the successful growth of BNNTs.[32] The G/D ratio of the bare SWCNT film and the SWCNT−BNNT heterostructured film did not change, which indicates that the crystalline structure of the SWCNT is well preserved after BNNT wrapping.

Thermal Conductance Measurement by IR Thermographic Method. To investigate the thermal properties of the SWCNT−BNNT heterostructured film, a contact-free steady-state IR thermography measurement was performed.[33] The experimental setup is briefly illustrated in Figure 3a. The SWCNT−BNNT film is dry-transferred from the graphite substrate and suspended between two silicon cantilevers fixed on a heat source and sink. The thermal image of silicon cantilevers and the sample is in the view of the IR camera through a ZnSe window (Figure 3b). The *x*-axis is denoted as the position along the silicon-film-silicon direction, and the *y*-direction is perpendicular to it. Because the sample is on a millimeter scale, the suspended film sample could be regarded as uniform, and the temperature perpendicular to the heat transport path at the same *x*-position could be treated as identical. Therefore, heat transport along the silicon−film−silicon direction can be regarded as quasi-one-dimensional, and the temperature profile is plotted in Figure 3b. Detailed calculation steps are shown in Supporting Information, Figure S4. The temperature along the *x*-axis is the average temperature of all *y*-points with the same *x*-value. A linear temperature distribution is observed for both the silicon cantilever and the suspended SWCNT−BNNT film. As the parts of the silicon cantilevers and the suspended samples that are in contact are on the macroscale, thermal contact resistance can be ignored in this study. Therefore, the temperature of the sample and silicon cantilevers at the contact parts can be regarded as the same value for further calculations.

As illustrated in Figure 3b, the heat transfer along the silicon−film−silicon is steady-state one-dimensional conduction, where the heat flux through the SWCNT−BNNT film and silicon cantilever satisfies the following equation

$$Q_{\text{silicon}} = Q_{\text{film}} \tag{1}$$

where "silicon" denotes the silicon cantilever and "film" denotes the SWCNT−BNNT film. By integrating Fourier's law into eq 1, it is further simplified to

$$\lambda_{\text{silicon}} \times \left[\left(\frac{\mathrm{d}T}{\mathrm{d}x}\right)_{\text{swi}} - \left(\frac{\mathrm{d}T}{\mathrm{d}x}\right)_{\text{swo}}\right]\cdot t_{\text{silicon}}\cdot W_{\text{silicon}} = \lambda_{\text{film}}\cdot\left(\frac{\mathrm{d}T}{\mathrm{d}x}\right)_{\text{film}}\cdot t_{\text{film}}\cdot W_{\text{film}} \tag{2}$$

In eq 2, λ, t, and W are the thermal conductivity, thickness, and width of the material denoted in the subscript, respectively, while "swi" and "swo" indicate silicon with and without sample film, respectively. The measurement of the unloaded pair of silicon cantilevers is used as a control experiment to remove the influence of radiation heat transfer. (Details are in Supporting Information.) Width of the silicon and the sample could be measured in the IR image, and the thickness of the silicon cantilever was 100 μm. The thermal conductivity of silicon is available from existing literature.[34,35] The temperature gradient is calculated by fitting the data points in Figure 3b. As the SWCNT−BNNT film is very thin and soft, the normal optical method and atomic force microscopy are not practical in determining the thickness of the sample. Therefore, instead of thermal conductance, the product of thermal conductivity and thickness, called sheet thermal conductance, was used, which is also commonly used in other studies.[36]

The Sheet Thermal Conductance of Pristine and Annealed SWCNT Films. The first step for CVD growth of BNNT is a heating step, and during this procedure, the suspended SWCNT template film first undergoes an annealing process at 1075 °C for 1 h. When annealed, a common phenomenon for CNT films, arrays, fibers, and mats is that CNTs tend to approach each other and form bundles, and the number of intertube contacts increases considerably.[19,37−39] This contact is believed to dramatically decrease thermal conductance and lead to phonon scattering.[40,41] To check the influence of the annealing procedure on the SWCNT film, the sheet thermal conductance of bare SWCNT films and annealed films were compared. First, the sheet thermal conductance of the bare SWCNT film was measured, and the result is plotted by black circles in Figure 4a. Then, annealed SWCNT samples were prepared by subjecting the SWCNT film to the same CVD method without ammonia borane, followed by the thermal conductance measurement. The result is plotted together with the result of the bare SWCNT film. As shown in Figure 4a, for bare films the sheet thermal conductance decreases as transparency increases, which is due to the decrease in the number of heat conduction paths (the number of SWCNTs) at high transparency, and the trend is consistent with previous research.[33,36] For all samples measured, the sheet thermal conductance shows decrease after annealing (orange triangle) compared with that of samples without treatment. The annealed sample of T92 films became too thin to perform dry transfer after annealing, so the value was not obtained. From the trend reflected by the other four samples, it is reasonable to speculate that the sheet thermal conductance of the T92 film also decreases compared with the original value. It is important to know what changes in the templates are caused by the experimental procedure before BNNT growth, which is helpful to correctly discuss the role that BNNT plays in the heterostructured film.

The Sheet Thermal Conductance of SWCNT−BNNT Heterostructured Films. The sheet thermal conductance values of SWCNT−BNNT films are plotted against the transparency as shown in Figure 4b together with the result of the annealed SWCNT films. For all samples, the sheet thermal conductance shows a clear enhancement after BNNT wrapping. This enhancement is attributed to the thermally conductive BNNTs[42−45] that coat the SWCNT film and act as additional thermal transport channels. The degree of increase is different for the samples measured and is plotted with blue hollow rhombuses in Figure 4b. The sample with higher transparency shows a larger increase compared with the thicker ones with lower transparency. The least amount of change was observed in the T53 film with only ∼24% improvement. For the T87 transparent sample, an ∼80% increase is achieved. Note that, along with sheet thermal conductance, thermal conductivity of SWCNT−BNNT films is also enhanced because the film thickness is assumed to be barely unchanged by BNNT growth (Supporting Information, Figure S7). The increase in the sheet thermal conductance of theT92 film after BNNT wrapping is approximately 93% compared with that of the bare SWCNT film before annealing (Supporting Information, Table S1). As stated in the last section, it is reasonable to predict an even larger increase if the sheet thermal conductance of the annealed T92 film could be measured. These varied increases could be explained from the following two perspectives. Because the original sheet thermal conductance of the low-transparency SWCNT film is relatively high, the contribution from additional heat-conducting channels offered by BNNTs becomes less prominent than in the other samples. The other explanation is the diameter of the BNNTs. For the T92 film, the density of SWCNTs is low, so bundles are formed with small diameters and are loosely packed with each other. Therefore, the diameter of BNNTs is also relatively small. However, the bundle size in the T53 film is larger than in the other samples, and the bundles are tightly packed, leading to a larger BNNT size. For 1D structures such as CNTs, the diameter has a reverse relationship with thermal conductance; that is, the smaller the diameter is, the higher the heat transport ability.[46] Consequently, the contribution from large-diameter BNNTs has a limited improvement in the overall performance for thick SWCNT films.

Another factor worth discussing is the effect of dedoping. SWCNT films are naturally *p*-doped by oxygen or other molecules adsorbed on the film.[47,48] During the vacuum annealing process, the adsorbed molecules are removed, and the film is purified. Consequently, the film is dedoped after annealing. This dedoping denotes an obvious change in electron density (details are in Supporting Information). Figure 4c shows the electrical conductance of the bare SWCNT film, the annealed SWCNT film, and the SWCNT−BNNT film. The dedoping effect caused an obvious change in the electrical conductance of the bare SWCNT film before and after annealing, while the difference between the annealed SWCNT film and the SWCNT−BNNT film was relatively small (Supporting Information). This indicates that the high electrical conductance of pristine SWCNT films is maintained even after the BNNT coating. With further study, the SWCNT−BNNT films are possibly used for electrical applications. The ratio of thermal conductance and electrical conductance (σ) gives an estimation of the electronic contribution to the thermal conductivity of the SWCNT film. The value of $\lambda/\sigma T$ at room temperature of the T87 SWCNT film is 2 orders of magnitude greater than that of the Lorenz number as determined by the Wiedemann−Franz law (details are in Supporting Information). Although the value of the Lorenz ratio calculated with experimental result differs among samples, the phenomenon holds true for all the samples measured, confirming the dominant role of phonons in thermal transport in SWCNT−BNNT films, which is consistent with previous studies on CNTs.[49,50]

Interpretation of the Enhanced Sheet Thermal Conductance. Thermal transport in this SWCNT−BNNT system is strongly influenced by its structure. A representative structural description is proposed in Figure 5. Two key components of the heterostructured film are enlarged to provide detailed information. Here, (I) is the isolated SWCNT wrapped by single-layer BNNT, and (II) is a junction of the template film coated by BN. Instead of separating the SWCNTs at the junction, BN forms a shell that wraps the junction and then extends along the SWCNTs and SWCNT bundles. From the morphology illustrated here, it is clear and reasonable to treat this heterostructured film as an inner SWCNT film and an outer BNNT network connected in parallel with each other.

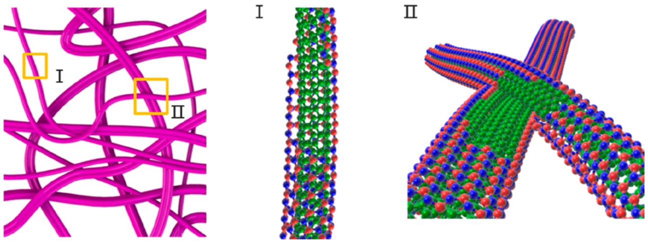

Figure 5. Typical network structure of the SWCNT−BNNT heterostructured film. Two representative segments of the heterostructured film indicated by I and II are enlarged for better observation of the outer and inner structure. In the enlarged images, BNNTs are partially omitted for clarity of the structure of inner SWCNTs. (I) A single-layer BNNT coating on an isolated SWCNT. (II) The BNNT formed at the SWCNT junction wraps the whole junction instead of separating the upper SWCNT from the lower SWCNT bundle.

To further discuss the thermal transport mechanism of the heterostructured film, a concise thermal resistance model was proposed in which the interaction between the BNNT and the inner SWCNT can be ignored, as the van der Waals force is very weak.[18] Therefore, the thermal resistance of the SWCNT film and the SWCNT−BNNT film could be separated into two parts

$$R_{\text{SWCNT film}} = R_{\text{junction}} + R_{\text{SWCNT}} \text{ and}$$
$$R_{\text{SWCNT−BNNT film}} = R_{\text{junction}} + R_{\text{SWCNT//BNNT}}$$

where R_{junction} is the thermal resistance caused by the contacts between SWCNTs in the film (Figure 5 (II)), R_{SWCNT} and $R_{\text{SWCNT//BNNT}}$ are the intrinsic thermal resistance of SWCNTs and the resistance of isolated SWCNTs and BNNT connected in parallel (Figure 5 (I)), respectively. Between these two resistances, R_{junction} is the major parameter that influences the total performance of a random network.[51] For very thin films, such as T92 and T87, the contact density is low, meaning that R_{junction} is small. Freely suspended SWCNTs between junctions are relatively long and form bundles with small diameters. BNNTs grown on these suspended SWCNs are also long and small in diameter. With the intrinsic high thermal conductivity of SWCNTs and BNNTs, a distinct enhancement of over 80% is observed for T87. In contrast, the high contact density of thicker template films led to larger values of R_{junction}, and the SWCNTs could only freely suspend between neighboring contacts. Additional layers of the BNNT coating reduces $R_{\text{SWCNT//BNNT}}$, but the minor proportion of this addition does not readily reduce the total thermal resistance; hence, the enhancement after BNNT wrapping is not obvious. In addition, high-temperature annealing during the CVD process creates more contacts in thicker SWCNT films than in thinner films and causes an even higher R_{junction}. This can be observed clearly from Figure 4a, where the drop in thermal conductance in the thicker film is evidently larger than in the thin films after annealing. On the basis of this situation, although the BNNT coating on SWCNTs in parallel decreases $R_{\text{SWCNT//BNNT}}$, the major contribution to the thermal resistance comes from the intertube contact R_{junction}, which cannot be lowered by the BNNT coating and even increases during the high-temperature process. Therefore, the sheet thermal conductance enhancement of samples with low transparency cannot reach that of samples with high transparency.

CONCLUSIONS

In summary, SWCNT−BNNT heterostructured films were successfully prepared by the CVD method utilizing SWCNT film templates. Then, a contact-free thermographic IR method was used to measure the sheet thermal conductance of the as-synthesized SWCNT−BNNT film. A comparison between the bare SWCNT film and the annealed films reveals the effect of the annealing procedure of CVD method on the samples. The enhancement in sheet thermal conductance proved the effectiveness of BNNTs in improving heat conduction, and a greater than 80% increase was achieved for the T87 film. Finally, a concise model is proposed to illustrate the mechanism of thermal transport in this system. This work provides information for tailoring heterostructured materials that can display additional unexpected properties in the future.

METHODS

Growth of BNNTs on the SWCNT Film Template. As the substrate, 1 mm thick graphite sheets were cut to 20 mm × 20 mm squares with a 10 mm × 10 mm window. The SWCNT film used in this work was synthesized by aerosol CVD.[25] The SWCNT film with filter paper was put on the substrate with the SWCNT film facing down and the filter paper facing up. By pushing the edges part, the SWCNT film made a tight connection with the graphite substrate. After removing the filter paper, the SWCNT film was released and was suspended on the graphite substrate for the following CVD process. Then, 30 mg of ammonia borane (H_3NBH_3) as the BNNT precursor was placed upstream relative to the sample and heated to 70−90 °C by a heating belt. Ar with 3% H_2 as the carrier gas flowed at a rate of 300 sccm. A low-pressure thermal CVD was used, which required that the reaction temperature and pressure be set as 1075 °C and 300 Pa, respectively. The number of external BNNT walls was influenced by the coating time. After 3 h of the CVD process, BNNTs were distributed evenly along the outer surface of most of the SWCNTs.

IR Thermographic Measurement. The IR camera used in this experiment is Avio H2640 with a resolution of 0.03 °C and detecting IR signal in the wavelength range from 8 to 14 μm. Emissivity is one important parameter needed to know the temperature of samples by IR camera. According to Kirchhoff's law, emissivity equals absorbance when the surface of the object can be approximated as a gray body. With FT-IR, the absorbance of all five SWCNT thin films and the silicon cantilever was measured. The absorbance of the silicon cantilever in this study was determined to be 0.94. While reading the temperature, the emissivity of the object should be in the range of 0.1 to 1 for the IR camera used. However, all five highly transparent SWCNT films used in this study possess an emissivity lower than 0.1. To obtain the temperature of the film, an equation was adopted by which the real temperature could be calculated from the nominal temperature measured at other emissivity values (Supporting Information, Figure S4). After BNNT growth on the film, the emissivity of the SWCNT−BNNT film was used for thermographic measurement.

ASSOCIATED CONTENT

Supporting Information

The Supporting Information is available free of charge at https://pubs.acs.org/doi/10.1021/acsnano.9b09754.

> Transparency of five SWCNT film template, optical photograph of bare SWCNT film, flexibility of SWCNT film, real temperature calculation, control experiment, discussion on electrical conductivity change, sheet resistance analysis, uncertainty analysis, Wiedemann−Franz law analysis, and estimation of thermal conductivity (PDF)

AUTHOR INFORMATION

Corresponding Authors

Shigeo Maruyama − *Department of Mechanical Engineering, The University of Tokyo, Bunkyo-ku, Tokyo 113-8656, Japan; Energy NanoEngineering Laboratory, National Institute of Advanced Industrial Science and Technology (AIST), Tsukuba 305-8654, Japan;* orcid.org/0000-0003-3694-3070; Email: maruyama@photon.t.u-tokyo.ac.jp

Taiki Inoue − *Department of Mechanical Engineering, The University of Tokyo, Bunkyo-ku, Tokyo 113-8656, Japan;* orcid.org/0000-0003-1739-917X; Email: inoue@photon.t.u-tokyo.ac.jp

Authors

Pengyingkai Wang − *Department of Mechanical Engineering, The University of Tokyo, Bunkyo-ku, Tokyo 113-8656, Japan;* orcid.org/0000-0001-7270-4320

Yongjia Zheng − *Department of Mechanical Engineering, The University of Tokyo, Bunkyo-ku, Tokyo 113-8656, Japan;* orcid.org/0000-0001-5836-6978

Rong Xiang − *Department of Mechanical Engineering, The University of Tokyo, Bunkyo-ku, Tokyo 113-8656, Japan;* orcid.org/0000-0002-4775-4948

Ahmed Shawky − *Department of Mechanical Engineering, The University of Tokyo, Bunkyo-ku, Tokyo 113-8656, Japan; Nanomaterials and Nanotechnology Department, Advanced Materials Division, Central Metallurgical R&D Institute (CMRDI), Cairo 11421, Egypt;* orcid.org/0000-0001-7590-8548

Makoto Watanabe − *Department of Mechanical Engineering, The University of Tokyo, Bunkyo-ku, Tokyo 113-8656, Japan*

Anton Anisimov − *Canatu, Ltd., Helsinki FI-00390, Finland*

Esko I. Kauppinen − *Department of Applied Physics, Aalto University School of Science, Aalto FI-00076, Finland;* orcid.org/0000-0003-1727-8810

Shohei Chiashi − *Department of Mechanical Engineering, The University of Tokyo, Bunkyo-ku, Tokyo 113-8656, Japan;* orcid.org/0000-0002-3813-0041

Complete contact information is available at: https://pubs.acs.org/10.1021/acsnano.9b09754

Author Contributions

P.W., T.I., and S.M. conceived the project. E.K. and A.A. synthesized the SWCNT films, and Y.Z. performed BNNT growth. P.W., R.X., and A.S. characterized the structure of the SWCNT−BNNT films. P.W and M.W. constructed the thermal conductance measurement setup. P.W. measured thermal conductance of the samples. P.W., T.I., S.C., and S.M. analyzed the data. P.W. and T.I. cowrote the manuscript. All the authors discussed the results and commented on the manuscript.

Notes

The authors declare no competing financial interest.

ACKNOWLEDGMENTS

Part of this work was financially supported by JSPS KAKENHI Grants JP15H05760, JP17K06187, JP17K14601, JP18H05329, and JP19H02543. Part of this work was supported by Laser Alliance, the University of Tokyo. Part of this work was supported by 316572 (CNTstress), the Academy of Finland. The authors would like to acknowledge support from S. Yotsumoto for the FT-IR experiment. The open molecular modeling platform SAMSON is used to build models.

REFERENCES

(1) Novoselov, K. S.; Mishchenko, A.; Carvalho, A.; Castro Neto, A. H. 2D Materials and van der Waals Heterostructures. *Science* **2016**, 353, No. aac9439.

(2) Shen, B.; Xie, H.; Gu, L.; Chen, X.; Bai, Y.; Zhu, Z.; Wei, F. Direct Chirality Recognition of Single-Crystalline and Single-Walled Transition Metal Oxide Nanotubes on Carbon Nanotube Templates. *Adv. Mater.* **2018**, *30*, 1803368.

(3) Liu, Y.; Weiss, N. O.; Duan, X.; Cheng, H.-C.; Huang, Y.; Duan, X. Van der Waals Heterostructures and Devices. *Nat. Rev. Mater.* **2016**, *1*, 16042.

(4) Alexeev, E. M.; Ruiz-Tijerina, D. A.; Danovich, M.; Hamer, M. J.; Terry, D. J.; Nayak, P. K.; Ahn, S.; Pak, S.; Lee, J.; Sohn, J. I.; Molas, M. R.; Koperski, M.; Watanabe, K.; Taniguchi, T.; Novoselov, K. S.; Gorbachev, R. V.; Shin, H. S.; Fal'ko, V. I.; Tartakovskii, A. I. Resonantly Hybridized Excitons in Moiré Superlattices in van der Waals Heterostructures. *Nature* **2019**, *567*, 81−86.

(5) Xiang, R.; Inoue, T.; Zheng, Y.; Kumamoto, A.; Qian, Y.; Sato, Y.; Liu, M.; Tang, D.; Gokhale, D.; Guo, J.; Hisama, K.; Yotsumoto, S.; Ogamoto, T.; Arai, H.; Kobayashi, Y.; Zhang, H.; Hou, B.; Anisimov, A.; Maruyama, M.; Miyata, Y.; et al. One-Dimensional van der Waals Heterostructures. *Science* **2020**, *367*, 537.

(6) Jing, L.; Tay, R. Y.; Li, H.; Tsang, S. H.; Huang, J.; Tan, D.; Zhang, B.; Teo, E. H. T.; Tok, A. I. Y. Coaxial Carbon@Boron Nitride Nanotube Arrays with Enhanced Thermal Stability and Compressive Mechanical Properties. *Nanoscale* **2016**, *8*, 11114−11122.

(7) Yuan, P.; Zhang, Z.; Yokokawa, S.; Zheng, Y.; Jin, L.; Set, S. Y.; Maruyama, S.; Yamashita, S. High Power Tolerant SWCNT−BNNT Saturable Absorber for Laser Mode-Locking. In *2019 Conference on Lasers and Electro-Optics (CLEO), Saturable Absorber Materials & Chalcogenides*, California, May 5−10, 2019; Derek, A., Ed.; IEEE: New York, 2019; SF3O.4, pp 1−2.

(8) Chen, C.-C.; Li, Z.; Shi, L.; Cronin, S. B. Thermoelectric Transport across Graphene/Hexagonal Boron Nitride/Graphene Heterostructures. *Nano Res.* **2015**, *8*, 666−672.

(9) Georgiou, T.; Jalil, R.; Belle, B. D.; Britnell, L.; Gorbachev, R. V.; Morozov, S. V.; Kim, Y.-J.; Gholinia, A.; Haigh, S. J.; Makarovsky, O.; Eaves, L.; Ponomarenko, L. A.; Geim, A. K.; Novoselov, K. S.; Mishchenko, A. Vertical Field-Effect Transistor Based on Graphene-WS_2 Heterostructures for Flexible and Transparent Electronics. *Nat. Nanotechnol.* **2013**, *8*, 100−103.

(10) Kang, K.; Lee, K.-H.; Han, Y.; Gao, H.; Xie, S.; Muller, D. A.; Park, J. Layer-by-Layer Assembly of Two-Dimensional Materials into Wafer-Scale Heterostructures. *Nature* **2017**, *550*, 229−233.

(11) Wu, C.-R.; Chang, X.-R.; Chu, T.-W.; Chen, H.-A.; Wu, C.-H.; Lin, S.-Y. Establishment of 2D Crystal Heterostructures by Sulfurization of Sequential Transition Metal Depositions: Preparation, Characterization, and Selective Growth. *Nano Lett.* **2016**, *16*, 7093−7097.

(12) Yang, W.; Chen, G.; Shi, Z.; Liu, C.-C.; Zhang, L.; Xie, G.; Cheng, M.; Wang, D.; Yang, R.; Shi, D.; Watanabe, K.; Taniguchi, T.; Yao, Y.; Zhang, Y.; Zhang, G. Epitaxial Growth of Single-Domain Graphene on Hexagonal Boron Nitride. *Nat. Mater.* **2013**, *12*, 792−797.

(13) Robinson, J. A. Growing Vertical in the Flatland. *ACS Nano* **2016**, *10*, 42−45.

(14) Zhang, H. Ultrathin Two-Dimensional Nanomaterials. *ACS Nano* **2015**, *9*, 9451−9469.

(15) Song, X.; Sun, J.; Qi, Y.; Gao, T.; Zhang, Y.; Liu, Z. Graphene/h-BN Heterostructures: Recent Advances in Controllable Preparation and Functional Applications. *Adv. Energy Mater.* **2016**, *6*, 1600541.

(16) He, T.; Li, T.; Huang, Z.; Tang, Z.; Guan, X. Mechanical and Thermal Properties of the Coaxial Carbon Nanotube@Boron Nitride Nanotube Composite. *Phys. E* **2019**, *107*, 182−186.

(17) Tay, R. Y.; Li, H.; Tsang, S. H.; Jing, L.; Tan, D.; Wei, M.; Teo, E. H. T. Facile Synthesis of Millimeter-Scale Vertically Aligned Boron Nitride Nanotube Forests by Template-Assisted Chemical Vapor Deposition. *Chem. Mater.* **2015**, *27*, 7156−7163.

(18) Jing, L.; Samani, M. K.; Liu, B.; Li, H.; Tay, R. Y.; Tsang, S. H.; Cometto, O.; Nylander, A.; Liu, J.; Teo, E. H. T.; Tok, A. I. Y. Thermal Conductivity Enhancement of Coaxial Carbon@Boron Nitride Nanotube Arrays. *ACS Appl. Mater. Interfaces* **2017**, *9*, 14555−14560.

(19) Feng, Y.; Inoue, T.; An, H.; Xiang, R.; Chiashi, S.; Maruyama, S. Quantitative Study of Bundle Size Effect on Thermal Conductivity of Single-Walled Carbon Nanotubes. *Appl. Phys. Lett.* **2018**, *112*, 191904.

(20) Pop, E.; Mann, D.; Wang, Q.; Goodson, K.; Dai, H. Thermal Conductance of an Individual Single-Wall Carbon Nanotube above Room Temperature. *Nano Lett.* **2006**, *6*, 96−100.

(21) Yoshino, K.; Kato, T.; Saito, Y.; Shitaba, J.; Hanashima, T.; Nagano, K.; Chiashi, S.; Homma, Y. Temperature Distribution and Thermal Conductivity Measurements of Chirality-Assigned Single-Walled Carbon Nanotubes by Photoluminescence Imaging Spectroscopy. *ACS Omega.* **2018**, *3*, 4352−4356.

(22) Yu, C.; Shi, L.; Yao, Z.; Li, D.; Majumdar, A. Thermal Conductance and Thermopower of an Individual Single-Wall Carbon Nanotube. *Nano Lett.* **2005**, *5*, 1842−1846.

(23) Cui, K.; Qian, Y.; Jeon, I.; Anisimov, A.; Matsuo, Y.; Kauppinen, E. I.; Maruyama, S. Scalable and Solid-State Redox Functionalization of Transparent Single-Walled Carbon Nanotube Films for Highly Efficient and Stable Solar Cells. *Adv. Energy Mater.* **2017**, *7*, 1700449.

(24) Qian, Y.; Jeon, I.; Ho, Y.-L.; Lee, C.; Jeong, S.; Delacou, C.; Seo, S.; Anisimov, A.; Kaupinnen, E. I.; Matsuo, Y.; Kang, Y.; Lee, H.-S.; Kim, D.; Delaunay, J.-J.; Maruyama, S. Multifunctional Effect of *p*-Doping, Antireflection, and Encapsulation by Polymeric Acid for High Efficiency and Stable Carbon Nanotube-Based Silicon Solar Cells. *Adv. Energy Mater.* **2020**, *10*, 1902389.

(25) Nasibulin, A. G.; Kaskela, A.; Mustonen, K.; Anisimov, A. S.; Ruiz, V.; Kivistö, S.; Rackauskas, S.; Timmermans, M. Y.; Pudas, M.; Aitchison, B.; Kauppinen, M.; Brown, D. P.; Okhotnikov, O. G.; Kauppinen, E. I. Multifunctional Free-Standing Single-Walled Carbon Nanotube Films. *ACS Nano* **2011**, *5*, 3214−3221.

(26) Moore, A. L.; Shi, L. Emerging Challenges and Materials for Thermal Management of Electronics. *Mater. Today* **2014**, *17*, 163−174.

(27) Golberg, D.; Bando, Y.; Tang, C. C.; Zhi, C. Y. Boron Nitride Nanotubes. *Adv. Mater.* **2007**, *19*, 2413−2432.

(28) Golberg, D.; Bando, Y.; Huang, Y.; Terao, T.; Mitome, M.; Tang, C.; Zhi, C. Boron Nitride Nanotubes and Nanosheets. *ACS Nano* **2010**, *4*, 2979−2993.

(29) Borowiak-Palen, E.; Pichler, T.; Fuentes, G. G.; Bendjemil, B.; Liu, X.; Graff, A.; Behr, G.; Kalenczuk, R. J.; Knupfer, M.; Fink, J. Infrared Response of Multiwalled Boron Nitride Nanotubes. *Chem. Commun.* **2003**, 82−83.

(30) Rubio, A.; Corkill, J. L.; Cohen, M. L. Theory of Graphitic Boron Nitride Nanotubes. *Phys. Rev. B: Condens. Matter Mater. Phys.* **1994**, *49*, 5081−5084.

(31) Xiang, H. J.; Yang, J.; Hou, J. G.; Zhu, Q. First-Principles Study of Small-Radius Single-Walled BN Nanotubes. *Phys. Rev. B: Condens. Matter Mater. Phys.* **2003**, *68*, 035427.

(32) Aydin, M. Vibrational and Electronic Properties of Single-Walled and Double-Walled Boron Nitride Nanotubes. *Vib. Spectrosc.* **2013**, *66*, 30−42.

(33) Feng, Y.; Inoue, T.; Watanabe, M.; Yoshida, S.; Qian, Y.; Xiang, R.; Kauppinen, E. I.; Chiashi, S.; Maruyama, S. Measurement of In-Plane Sheet Thermal Conductance of Single-Walled Carbon Nanotube Thin Films by Steady-State Infrared Thermography. *Jpn. J. Appl. Phys.* **2018**, *57*, 075101.

(34) Shanks, H. R.; Maycock, P. D.; Sidles, P. H.; Danielson, G. C. Thermal Conductivity of Silicon from 300 to 1400 K. *Phys. Rev.* **1963**, *130*, 1743−1748.

(35) Glassbrenner, C. J.; Slack, G. A. Thermal Conductivity of Silicon and Germanium from 3 K to the Melting Point. *Phys. Rev.* **1964**, *134*, A1058−A1069.

(36) Yoshida, S.; Feng, Y.; Delacou, C.; Inoue, T.; Xiang, R.; Kometani, R.; Chiashi, S.; Kauppinen, E. I.; Maruyama, S. Morphology Dependence of the Thermal Transport Properties of Single-Walled Carbon Nanotube Thin Films. *Nanotechnology* **2017**, *28*, 185701.

(37) Thess, A.; Lee, R.; Nikolaev, P.; Dai, H.; Petit, P.; Robert, J.; Xu, C.; Lee, Y. H.; Kim, S. G.; Rinzler, A. G.; Colbert, D. T.; Scuseria, G. E.; Tománek, D.; Fischer, J. E.; Smalley, R. E. Crystalline Ropes of Metallic Carbon Nanotubes. *Science* **1996**, *273*, 483.

(38) Hennrich, F.; Lebedkin, S.; Malik, S.; Tracy, J.; Barczewski, M.; Rösner, H.; Kappes, M. Preparation, Characterization and Applications of Free-Standing Single Walled Carbon Nanotube Thin Films. *Phys. Chem. Chem. Phys.* **2002**, *4*, 2273−2277.

(39) Ma, W.; Song, L.; Yang, R.; Zhang, T.; Zhao, Y.; Sun, L.; Ren, Y.; Liu, D.; Liu, L.; Shen, J.; Zhang, Z.; Xiang, Y.; Zhou, W.; Xie, S. Directly Synthesized Strong, Highly Conducting, Transparent Single-Walled Carbon Nanotube Films. *Nano Lett.* **2007**, *7*, 2307−2311.

(40) Prasher, R. S.; Hu, X. J.; Chalopin, Y.; Mingo, N.; Lofgreen, K.; Volz, S.; Cleri, F.; Keblinski, P. Turning Carbon Nanotubes from Exceptional Heat Conductors into Insulators. *Phys. Rev. Lett.* **2009**, *102*, 105901.

(41) Hu, L.; McGaughey, A. J. H. Thermal Conductance of the Junction between Single-Walled Carbon Nanotubes. *Appl. Phys. Lett.* **2014**, *105*, 193104.

(42) Chang, C. W.; Fennimore, A. M.; Afanasiev, A.; Okawa, D.; Ikuno, T.; Garcia, H.; Li, D.; Majumdar, A.; Zettl, A. Isotope Effect on the Thermal Conductivity of Boron Nitride Nanotubes. *Phys. Rev. Lett.* **2006**, *97*, 085901.

(43) Zhi, C.; Bando, Y.; Tang, C.; Golberg, D. Boron Nitride Nanotubes. *Mater. Sci. Eng., R* **2010**, *70*, 92−111.

(44) Xiao, Y.; Yan, X. H.; Cao, J. X.; Ding, J. W.; Mao, Y. L.; Xiang, J. Specific Heat and Quantized Thermal Conductance of Single-Walled Boron Nitride Nanotubes. *Phys. Rev. B: Condens. Matter Mater. Phys.* **2004**, *69*, 205415.

(45) Zhi, C.; Bando, Y.; Terao, T.; Tang, C.; Kuwahara, H.; Golberg, D. Towards Thermoconductive, Electrically Insulating Polymeric Composites with Boron Nitride Nanotubes as Fillers. *Adv. Funct. Mater.* **2009**, *19*, 1857−1862.

(46) Wang, P.; Xiang, R.; Maruyama, S., Thermal Conductivity of Carbon Nanotubes and Assemblies. In *Advances in Heat Transfer*; Sparrow, E. M., Abraham, J. P., Gorman, J. M., Eds.; Elsevier: New York, 2018; pp 43−122.

(47) Collins, P. G.; Bradley, K.; Ishigami, M.; Zettl, A. Extreme Oxygen Sensitivity of Electronic Properties of Carbon Nanotubes. *Science* **2000**, *287*, 1801.

(48) Kang, D.; Park, N.; Ko, J.-h.; Bae, E.; Park, W. Oxygen-Induced *p*-Type Doping of a Long Individual Single-Walled Carbon Nanotube. *Nanotechnology* **2005**, *16*, 1048−1052.

(49) Huang, H.; Liu, C. H.; Wu, Y.; Fan, S. Aligned Carbon Nanotube Composite Films for Thermal Management. *Adv. Mater.* **2005**, *17*, 1652−1656.

(50) Hone, J.; Whitney, M.; Piskoti, C.; Zettl, A. Thermal Conductivity of Single-Walled Carbon Nanotubes. *Phys. Rev. B: Condens. Matter Mater. Phys.* **1999**, *59*, R2514−R2516.

(51) Volkov, A. N.; Zhigilei, L. V. Scaling Laws and Mesoscopic Modeling of Thermal Conductivity in Carbon Nanotube Materials. *Phys. Rev. Lett.* **2010**, *104*, 215902.